Optically driven quantum networks: Applications in molecular electronics

H. Körner and G. Mahler
Institut für Theoretische Physik, Universität Stuttgart, Pfaffenwaldring 57, 7000 Stuttgart 80, Germany
(Received 29 June 1992; revised manuscript received 1 March 1993)

Progress in nanostructuring tends to provide us with synthetic structures for which, for example, energy or time scales can be adjusted in such a way that quantum systems with unusual physical properties emerge. The challenge of molecular electronics is to make these properties represent computer functions. We investigate a quantum network model consisting of a modular array of localized few-level subsystems. When driven optically, a diagonal (energy renormalizing) interaction among these subsystems is shown to lead to a complex stochastic dynamics, which may be interpreted as a highly parallel Monte-Carlo-type simulation "programmed" by the external light field. A first application is demonstrated in terms of a two-dimensional kinetic Ising model with $J(\mathbf{R}_n-\mathbf{R}_m)\sim|\mathbf{R}_n-\mathbf{R}_m|^{-3}$. In another application the nonlocal nonlinear optical properties are exploited in specific pump and probe scenarios: Under certain conditions simple image processing tasks are performed. A possible realization of such quantum network models by an array of charge-transfer quantum dots is discussed.

I. INTRODUCTION

The last decade has seen a large number of concepts being proposed within the field of molecular electronics. Although a precise definition of molecular electronics is still lacking, many researchers agree[1] that it should deal with information storage and processing on the molecular level, i.e., it should use nm-scale systems as basic structural elements (e.g., atoms, molecules, quantum dots) and excitations within these elements (e.g., electronic or structural) as information carriers. Such information processing will thus have to be described by the laws of quantum dynamics.

Other concepts simply try to implement conventional electronics on the molecular level: Proposals have been made to use molecular chains as wires[2,3] or complex molecules as switches[3,4] or diodes.[5] The fundamental difficulty of this approach is to realize a specific function within the constrained dynamical behavior of a nm-sized system having only few degrees of freedom. The dynamics of conventional electronic devices is described on the hydrodynamical level and fluctuations are not desirable. Simple scaling down increases noise and finally terminates in a quantum dynamical description with its probabilistic aspects. This quantum noise would severely limit the function of conventional electronic devices. Also the final step, the assemblage of molecular devices to a "molecular computer" and the connection to a macroscopic environment is still unsolved.[6] For many reasons, one may thus come to the conclusion that molecular electronics cannot simply be conventional electronics with other materials on other length scales: To be competitive, molecular electronics should particularly overcome disadvantages of the conventional von Neumann computer architecture, e.g., the lack of a massive parallelism. The idea of networks is promising in this connection. However, concepts such as neural nets,[7] parallel algorithms,[8] and deterministic cellular automata[9] only define abstract rules: The implementation on the molecular level has to deal with difficulties similar to those discussed above. On the other hand, synthetic quantum networks that have been realized so far, e.g., with quantum point contacts[10] or in doped zeolite crystals,[11] do not seem to support any computer function. It seems that a central paradigm of computational science, the independence of computer concepts from their realization, will be violated in molecular electronics.

Our model of an optically driven quantum network shows, indeed, this close connection between computer conception and physical implementation. The quantum network consists of an array of local quantum objects (e.g., functional molecules or quantum dots) as network nodes. Network links are realized by a physical interaction between these nodes. Network dynamics is induced by an external light field. We exploit the inherent stochastics of quantum dynamics instead of considering it as a noise source to be suppressed. We show that the connection between physical measurement (absorption) and external control parameters (pump light field) can be directly interpreted as a computer function. The task of nanostructuring is to adjust the network parameters (i.e., energy scales, transition rates) in such a way that "programming" this computer function (realized also by external control fields), at least in a restricted manner, is possible. Partial aspects of this quantum network idea have already been demonstrated experimentally: Single quantum objects such as ions in a Paul trap[12–14] or defects in a solid matrix[15] can be controlled by the light field.[16] Interactions between individual quantum objects—essential for a cooperative network dynamics—have been demonstrated for the defect in the matrix system[17] or, even more pertinent, between individual trap states in small tunnel junctions.[18] These phenomena, so far, have never been optimized for the realization of a "useful" quantum network. Here, we propose a charge-transfer quantum-dot array as a prototype system.

A trivial version of a quantum network would consist

 ©1993 The American Physical Society

of an ensemble of independent nodes. This leads to a typical absorption spectrum as observed, e.g., for an ensemble of defects in a solid matrix. A simple transfer interaction between nodes with a single quantum state leads to another trivial case, the ideal one-band crystal. Obviously, a certain complexity of the network is required to get a functional device. In our model, this is realized by a three-state node with a hierarchy of transition rates and a dipole-dipole interaction between the nodes.

Our paper is organized as follows: In Sec. II we develop the general network model and describe its dynamics in the external light field and its optical properties. In Sec. III the network model is specified and a possible realization is presented. Preliminary applications in molecular electronics are demonstrated in Sec. IV. Finally, in Sec. V, we summarize and discuss our results.

II. NETWORK MODEL

A. Network Hamiltonian

Our quantum network is a modular system in the sense that it is composed of identical primitive subsystems. The subsystem ("network node") is taken to be a quantum-mechanical few-level system. The interaction between these nodes forms the "network links."

The network Hamiltonian for N interacting subsystems can thus be written as

$$\hat{H}=\sum_{n=1}^{N}\hat{H}_n+\tfrac{1}{2}\sum_{\substack{n,m=1\\ n\neq m}}^{N}\hat{H}_{nm} \ . \tag{2.1}$$

Each isolated subsystem n is an I-level system defined by

$$\hat{H}_n=\sum_{i_n=1}^{I}E^0_{i_n}|i_n\rangle\langle i_n| \ . \tag{2.2}$$

In "natural" quantum networks (e.g., crystals), typical interactions are, e.g., the single-particle transfer

$$\hat{H}_{nm}=\sum_{i_n,i_m=1}^{I}V^{nm}_{i_n i_m}|i_n\rangle\langle i_m| \tag{2.3}$$

or the so-called Förster-mechanism[19]

$$\hat{H}_{nm}=\sum_{\substack{i_n,j_n=1\\ i_n\neq j_n}}^{I}\sum_{\substack{i_m,j_m=1\\ i_m\neq j_m}}^{I}V^{nm}_{i_n j_n i_m j_m}|i_n,i_m\rangle\langle j_n,j_m| \tag{2.4}$$

leading to delocalized Bloch states. Here we consider instead the following energy renormalization:

$$\hat{H}_{nm}=\sum_{i_n,i_m=1}^{I}V^{nm}_{i_n i_m}|I_n,i_m\rangle\langle i_n,i_m| \ . \tag{2.5}$$

Without loss of generality we set $V^{nm}_{i_n i_m}=V^{mn}_{i_m i_n}$. This diagonal interaction is generic for a complex optically driven network dynamics. The product states

$$|\{i_n\}\rangle=|i_1,i_2,\ldots,i_N\rangle=|i_1\rangle\otimes|i_2\rangle\otimes\cdots\otimes|i_N\rangle \tag{2.6}$$

that form a $M=I^N$-dimensional basis in the state space of the network remain eigenstates of the network Hamiltonian (2.1):

$$\hat{H}|\{i_n\}\rangle=E_{\{i_n\}}|\{i_n\}\rangle \ . \tag{2.7}$$

They are localized states, as opposed to the situation of natural quantum networks. The corresponding eigenvalues are

$$E_{\{i_n\}}=\sum_{n=1}^{N}E^0_{i_n}+\tfrac{1}{2}\sum_{\substack{n,m=1\\ n\neq m}}^{N}V^{nm}_{i_n i_m} \ . \tag{2.8}$$

We assume the following hierarchy in the energy scales

$$V^{nm}_{ij}\ll|E^0_k-E^0_l| \quad \text{for all } i,j,n,m,k,l \tag{2.9}$$

that leads to a certain grouping of the levels in energy space and will allow for a specific control by the optical driving field.

B. Driven quantum systems

In this section, we consider an arbitrary M-level system coupled to a heat bath and to external (pump and probe) light fields. Its dynamics is described by a generalized master equation for the reduced density matrix,[20]

$$\begin{aligned}\frac{d}{dt}\rho_{ij}(t)=&-i\omega_{ij}\rho_{ij}(t)+\frac{i}{\hbar}E(t)\sum_{k=1}^{M}[d_{ik}\rho_{kj}(t)\\ &-d_{kj}\rho_{ik}(t)]\\ &+\delta_{ij}\sum_{k=1}^{M}[W_{ik}\rho_{kk}(t)-W_{ki}\rho_{ii}(t)]\\ &-(1-\delta_{ij})\gamma_{ij}\rho_{ij}(t) \ .\end{aligned} \tag{2.10}$$

The interaction with the external light field $E(t)$ is considered here in the dipole approximation, $\hbar\omega_{ij}=E_i-E_j$ is the transition energy between states i and j, and $d_{ij}=\langle i|\hat{d}|j\rangle$ the transition dipole moment. For simplicity, $E(t)$ and d_{ij} are treated as scalar quantities. The heat-bath coupling shows up in the transition rates W_{ik} from state k to state i and the phase relaxation rates $\gamma_{ij}=\gamma_{ji}$.

The external light field $E(t)$ is composed of two parts:

$$E(t)=E_{\text{pump}}(t)+E_{\text{probe}}(t) \ , \tag{2.11}$$

where

$$|E_{\text{probe}}(t)|\ll|E_{\text{pump}}(t)| \ . \tag{2.12}$$

The strong pump field E_{pump} induces the dynamics in the M-level system, whereas the weak probe light field E_{probe} will be used to obtain information about this dynamics. This may be accomplished, e.g., by measuring the absorption of the probe beam.

We now apply a perturbation expansion to the reduced density matrix[21] up to first order in the probe field:

$$\rho_{ij}(t)=\rho^{(0)}_{ij}(t)+\rho^{(1)}_{ij}(t)+\cdots \ . \tag{2.13}$$

The zeroth-order dynamics $\rho^{(0)}(t)$ is then given by Eq. (2.10) with $E(t)=E_{\text{pump}}(t)$. For reasons that will be explained below, we use a stationary and incoherent pump field (with a spectral band width $\gg\gamma_{ij}$). The generalized

master equation (2.10) then reduces to a simple Pauli master equation (rate equation) for the diagonal elements:[22]

$$\frac{d}{dt}\rho_{ii}^{(0)}(t)=\sum_{k=1}^{M}\left[R_{ik}\rho_{kk}^{(0)}(t)-R_{ki}\rho_{ii}^{(0)}(t)\right], \tag{2.14}$$

with total (effective) transition rates

$$R_{ik}=W_{ik}+B_{ik}U_{\text{pump}}(\omega_{ik}) . \tag{2.15}$$

Here, $B_{ik}=B_{ki}=\pi|d_{ik}|^2/(3\hbar^2\epsilon_0)$ is the respective Einstein B coefficient and $U_{\text{pump}}(\omega)=U_{\text{pump}}(-\omega)=2\epsilon_0|E_{\text{pump}}(\omega)|^2$ the spectral energy density of the pump field.

In the following, we will restrict ourselves to stationary conditions. Information about the pump-induced state may be deduced from the expectation value of an observable $\hat{A}$:

$$\langle\hat{A}\rangle=\text{tr}(\hat{\rho}^{(0)}\hat{A})=\sum_{i=1}^{M}\rho_{ii}^{(0)}A_{ii} , \tag{2.16}$$

with $A_{ii}=\langle i|\hat{A}|i\rangle$. $\rho_{ii}^{(0)}$ is the stationary solution of Eq. (2.14).

More detailed information will be delivered by the response to the probe field. The first-order response is determined by

$$\begin{aligned}\frac{d}{dt}\rho_{ij}^{(1)}(t)=&-i\omega_{ij}\rho_{ij}^{(1)}(t)\\&+\delta_{ij}\sum_{k=1}^{M}\left[W_{ik}\rho_{kk}^{(1)}(t)-W_{ki}\rho_{ii}^{(1)}(t)\right]\\&-(1-\delta_{ij})\gamma_{ij}\rho_{ij}^{(1)}(t)\\&+\frac{i}{\hbar}E_{\text{probe}}(t)d_{ij}\left[\rho_{jj}^{(0)}(t)-\rho_{ii}^{(0)}(t)\right] .\end{aligned} \tag{2.17}$$

We assume that the stationary probe field can be decomposed into Fourier components according to

$$E_{\text{probe}}(t)=\sum_{\omega}E_{\text{probe}}(\omega)\exp(i\omega t) . \tag{2.18}$$

With the same decomposition for the nondiagonal elements

$$\rho_{ij}^{(1)}(t)=\sum_{\omega}\rho_{ij}^{(1)}(\omega)\exp(i\omega t) , \tag{2.19}$$

we get from (2.17)

$$\rho_{ij}^{(1)}(\omega)=\frac{E_{\text{probe}}(\omega)d_{ij}}{\hbar(\omega+\omega_{ij}-i\gamma_{ij})}\left[\rho_{jj}^{(0)}-\rho_{ii}^{(0)}\right] . \tag{2.20}$$

Optical properties (absorption and dispersion of the probe beam) are described by a nonlinear susceptibility $\chi(\omega)$. The Fourier component of the polarization is given by

$$P(\omega)=\frac{1}{V}\text{tr}\left[\hat{\rho}^{(1)}(\omega)\hat{d}\right]=\frac{1}{V}\sum_{i,j=1}^{M}\rho_{ij}^{(1)}(\omega)d_{ji} . \tag{2.21}$$

V is the volume of the system. $\chi(\omega)$ is then defined as

$$\begin{aligned}\chi(\omega)=&\frac{1}{\epsilon_0}\frac{P(\omega)}{E_{\text{probe}}(\omega)}\\=&\frac{1}{\hbar\epsilon_0 V}\sum_{i,j=1}^{M}\frac{|d_{ij}|^2(\omega+\omega_{ij}+i\gamma_{ij})}{(\omega+\omega_{ij})^2+\gamma_{ij}^2}\left[\rho_{jj}^{(0)}-\rho_{ii}^{(0)}\right] .\end{aligned} \tag{2.22}$$

It describes the linear response to the probe field, but nevertheless is called nonlinear, since it depends on the pump field via $\rho_{kk}^{(0)}$: The probe field thus measures the occupation difference $\rho_{jj}^{(0)}-\rho_{ii}^{(0)}$ induced by the pump field: $\chi'(\omega)=\text{Re}[\chi(\omega)]$ is the dispersion and $\chi''(\omega)=-\text{Im}[\chi(\omega)]$ the absorption of the probe beam.

C. Application to the network Hamiltonian

The formalism developed in Sec. II B is now applied to the network $M=I^N$-level system with its eigenstates (2.6) and energies (2.8). The single indices i in the corresponding equations, then, just stand for the whole set $\{i_n\}$, characterizing the state of the network. The equations can be simplified if one takes into account that the parameters W_{ij}, B_{ij}, R_{ij}, and d_{ij} are zero unless the states $i=\{i_n\}$ and $j=\{j_n\}$ differ in one position at most, i.e., $\{i_n\}=\{i_1,\ldots,i_{m-1},i_m,i_{m+1},\ldots,i_N\}$ and $\{j_n\}=\{i_1,\ldots,i_{m-1},j_m,i_{m+1},\ldots,i_N\}$: This is due to the fact that the underlying transition operators are single-particle operators. From Eq. (2.8) we get

$$\begin{aligned}\hbar\omega_{i_m j_m}(\{i_n\})=&E_{\{i_1,i_2,\ldots,i_{m-1},i_m,i_{m+1},\ldots,i_N\}}\\&-E_{\{i_1,i_2,\ldots,i_{m-1},j_m,i_{m+1},\ldots,i_N\}}\\=&\hbar\omega_{i_m j_m}^0+\sum_{\substack{n=1\\n\neq m}}^{N}(V_{i_m i_n}^{mn}-V_{j_m i_n}^{mn}) ,\end{aligned} \tag{2.23}$$

which can be interpreted as a renormalized transition energy between the states i_m and j_m of subsystem m, depending on the neighborhood $\{i_n\}$, $n\neq m$. $\hbar\omega_{i_m j_m}^0=E_{i_m}^0-E_{j_m}^0$ is the transition energy for the isolated subsystem. Then, the pump dynamics (2.14) of the quantum network is described by the rate equation

$$\begin{aligned}\frac{d}{dt}\rho^{(0)}(i_1,i_2,\ldots,i_N;t)=\sum_{m=1}^{N}\sum_{j_m=1}^{I}&[R_{i_m j_m}(\{i_n\})\rho^{(0)}(i_1,i_2,\ldots,i_{m-1},j_m,i_{m+1},\ldots,i_N;t)\\&-R_{j_m i_m}(\{i_n\})\rho^{(0)}(i_1,i_2,\ldots,i_{m-1},i_m,i_{m+1},\ldots,i_N;t)] .\end{aligned} \tag{2.24}$$

$\rho^{(0)}(\{i_n\};t)=\rho_{\{i_n\}\{i_n\}}^{(0)}(t)$ is a diagonal element of the $M=I^N$-dimensional network density matrix. The total rate for the transition $j_m\to i_m$ in subsystem m is given by

$$R_{i_m j_m}(\{i_n\}) = W_{i_m j_m} + B_{i_m j_m} U_{\text{pump}}[\omega_{i_m j_m}(\{i_n\}), m] \,. \tag{2.25}$$

$U_{\text{pump}}(\omega, m)$ is the local pump-energy density at site m. The fact that the transition rate $R_{i_m j_m}(\{i_n\})$ depends on the state of the other subsystems is the origin of a complex network dynamics: If the spectral energy density $U_{\text{pump}}(\omega, m)$ was a constant with respect to ω or the interaction between the subsystems vanished, the transition rate would not depend on the neighborhood: The coupled dynamics (2.24) would then reduce to a system of independent rate equations for each subsystem.

The expectation value of a local observable $\hat{A}_m$ is given by

$$\langle \hat{A}_m \rangle = \sum_{\{i_n = 1\}}^{I} \rho^{(0)}(\{i_n\}) A_{i_m i_m} \,, \tag{2.26}$$

with $A_{i_m i_m} = \langle i_m | \hat{A}_m | i_m \rangle$.

$$\langle \hat{A} \rangle = \sum_{m=1}^{N} \langle \hat{A}_m \rangle \tag{2.27}$$

is the expectation value of the total quantity $\hat{A}$.

From Eq. (2.22) we derive that the susceptibility

$$\chi(\omega) = \frac{1}{N} \sum_{m=1}^{N} \chi(\omega, m) \tag{2.28}$$

of the network is the mean value of the local susceptibility

$$\chi(\omega, m) = \frac{1}{\hbar \epsilon_0 v} \sum_{i_m, j_m = 1}^{I} \sum_{\substack{\{i_n = 1\} \\ n \neq m}}^{I} \frac{|d_{i_m j_m}|^2 [\omega + \omega_{i_m j_m}(\{i_n\}) + i\gamma_{i_m j_m}]}{[\omega + \omega_{i_m j_m}(\{i_n\})]^2 + \gamma_{i_m j_m}^2} \times [\rho^{(0)}(i_1, \ldots, j_m, \ldots, i_N) - \rho^{(0)}(i_1, \ldots, i_m, \ldots, i_N)] \,. \tag{2.29}$$

$v = V/N$ is the volume of a single subsystem. In contrast to a subsystem in a static environment where each transition $i_m \leftrightarrow j_m$ contributes a single Lorentzian to the absorption spectrum ("homogeneous line"),[15] we get here a superposition of several lines. This inhomogeneous line arises because the environment of subsystem m that is built up here by all other subsystems $n \neq m$ explicitly occurs at the dynamics. Similar effects have recently been observed as spectral jumps in the resonance frequency of a single pentacene defect in a p-terphenyl crystal.[17]

The assumption of an incoherent pump field has led to a dynamical description in the form of a rate equation (2.24) instead of a generalized master equation (2.10). The great advantage now is that Monte Carlo simulation provides an effective numerical method to determine the properties of rate-equation dynamics in a high-dimensional-state space. No comparably effective method exists for a generalized master equation. The Monte Carlo method simulates a Markoff process $\{i_n(t)\}$ defined by the transition rates (2.25). The stationary solution $\rho^{(0)}(\{i_n\})$ of the rate equations (2.24) is then given by the time average

$$\rho^{(0)}(\{i_n\}) = \lim_{t_{\max} \to \infty} \frac{1}{t_{\max}} \int_0^{t_{\max}} dt \prod_{n=1}^{N} \delta_{i_n, i_n(t)} \,. \tag{2.30}$$

Inserting (2.30) in (2.29) and (2.26) gives the following expressions for the susceptibility $\chi(\omega, m)$ and the expectation value $\langle \hat{A}_m \rangle$:

$$\chi(\omega, m) = \lim_{t_{\max} \to \infty} \frac{1}{\hbar \epsilon_0 v} \frac{1}{t_{\max}} \int_0^{t_{\max}} dt \sum_{i_m, j_m = 1}^{I} \frac{|d_{i_m j_m}|^2 (\omega + \omega_{i_m j_m}[\{i_n(t)\}] + i\gamma_{i_m j_m})}{(\omega + \omega_{i_m j_m}[\{i_n(t)\}])^2 + \gamma_{i_m j_m}^2} [\delta_{j_m, i_m(t)} - \delta_{i_m, i_m(t)}] \tag{2.31}$$

and

$$\langle \hat{A}_m \rangle = \lim_{t_{\max} \to \infty} \frac{1}{t_{\max}} \int_0^{t_{\max}} dt \; A_{i_m(t) i_m(t)} \,. \tag{2.32}$$

The integrand in Eq. (2.31) may be interpreted as a time-dependent spectrum where the resonance frequencies $\omega_{i_m j_m}[\{i_n(t)\}]$ evolve as a random telegraph signal. The experimental observation of such spectral jumps[17] suggests that the Monte Carlo simulation, here, is not only an effective numerical method, but even constitutes the "real dynamics."[23] This view of quantum dynamics of open systems as inherently stochastic is confirmed in various other experiments from different fields: Quantum jumps in the fluorescence of single ions [12, 13, 14] or current fluctuations in very small electronic devices [24] are pertinent examples.

III. NETWORK REALIZATION

The realization of the quantum network model requires a complex structure on the atomic scale. Technologies for structural control on this level are in the process of development: Three-dimensional semiconductor nanostructuring and, starting from the opposite direction, the chemical synthesis and (self-) assembly of functional molecules are promising approaches.

The basic element (subsystem) of our network model is an optically controllable charge-transfer center. Prototype structures that realize this network node would be, e.g., charge-transfer quantum dots[25] or donor-acceptor-modified molecular chains.[3,4,26] Both systems can be described by a minimal $I=3$-level system (Fig. 1).[25,27] The horizontal axis symbolizes electronic or structural coordinates, depending on the realization of the model. The different spatial localization behavior of the states i results in different static dipole moments $d_{ii}=\langle i|\hat{d}|i\rangle$ that characterize the charge transfer.

In the following we will restrict ourselves to a two-dimensional square array of identical charge-transfer quantum dots as shown in Fig. 2.[28] Indeed, such charge-transfer quantum dots are not yet under experimental control. However, two-dimensional quantum-well structures of that type[29] or simpler zero-dimensional quantum dots[30] have already been realized.

We specify the dipole moments d_{ii} by[31]

$$d_{22}=-d_{11}=d\ ,\quad d_{33}=0\ . \tag{3.1}$$

The specific localization behavior is responsible also for a hierarchy in the transition rates W_{ij} (Ref. 25)

$$W_{21},W_{12}\ll W_{13},W_{23} \tag{3.2}$$

that stabilizes the charge transfer. These rates arise from an interaction with the (e.g., photon or phonon) heat bath. For simplicity we assume its temperature $k_BT\ll\hbar\omega_{31},\hbar\omega_{32}$, so that

$$W_{31},W_{32}\ll W_{13},W_{23} \tag{3.3}$$

also holds. The dominant part of the intersubsystem interaction is the static (diagonal) dipole-dipole interaction.[31] For dipole moments d_{ii} perpendicular to the connecting line $\mathbf{R}_m-\mathbf{R}_n$, we get for Eq. (2.5)

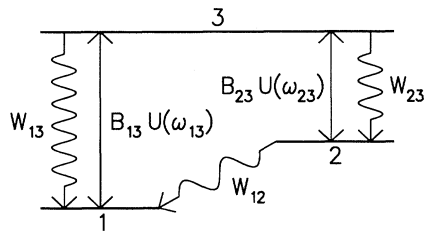

FIG. 1. Driven three-level system: Minimal model for a controllable charge-transfer center. Transitions are induced by heat-bath coupling (rate W_{ik}) and external light field [rate $B_{ik}U(\omega_{ik})$].

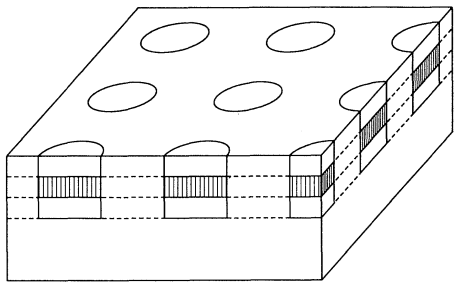

FIG. 2. Charge-transfer quantum-dot array: Possible realization for a synthetic quantum network. The single three-layered dot represents an asymmetric double-well potential in the valence and conducting bands so that a spectrum as in Fig. 1 results (Ref. 25).

$$V_{i_ni_m}^{nm}=\frac{d_{i_ni_n}d_{i_mi_m}}{4\pi\epsilon\epsilon_0|\mathbf{R}_n-\mathbf{R}_m|^3}\ . \tag{3.4}$$

This static dipole-dipole coupling is the first term in the multipole expansion of the intersubsystem Coulomb interaction.[31] Other types of interactions, such as single-particle transfer or dynamic (nondiagonal) dipole-dipole interaction (Förster transfer), can be neglected here for two reasons: First, the network lattice constant ($a\approx 100$ nm for the model in Ref. 31) is large compared to natural networks (crystals). Second, the diagonal interaction eliminates degeneracy, which is a condition for an effective transfer process. The local picture (2.6) thus remains valid.[32]

Typical orders of magnitude for the transition energies are[25]

$$\begin{aligned}&\hbar\omega_{31}\approx\hbar\omega_{32}\approx 1\text{ eV}\ ,\\&\hbar\omega_{21}\approx 10\text{ meV}\ ,\end{aligned} \tag{3.5}$$

and for the dipole-dipole interaction $\hbar C_0$ (see below) between two nearest neighbors n and m (Ref. 31)

$$\hbar C_0=V_{11}^{nm}=V_{22}^{nm}=-V_{12}^{nm}=-V_{21}^{nm}=\frac{d^2}{4\pi\epsilon\epsilon_0a^3}\approx 0.01\text{ meV}\ . \tag{3.6}$$

Thus the hierarchy (2.9) is fulfilled in this model system.

IV. RESULTS

A. The isolated subsystem

It might be helpful to first investigate the photodynamics of an isolated subsystem. An external light field couples the ground state 1 and the metastable state 2 with the transient state 3 and controls the charge-transfer dynamics (see Fig. 1). In the following we will study this dynamic with the formalism developed in Sec. II B. We assume that the rates of the light-induced transitions $1\leftrightarrow 3$ and $2\leftrightarrow 3$ lie within the range

$$W_{31},W_{32},W_{21},W_{12}\ll B_{ij}U_{\text{pump}}(\omega_{ij}^0)\ll W_{13},W_{23} \tag{4.1}$$

for $ij=13$, 31, 23, and 32. A direct light-field coupling $1\leftrightarrow 2$ can be neglected because of the negligible overlap of the corresponding states. Equations (4.1) and (3.3) lead to the following hierarchy in the total transition rates R_{ij} (2.15):

$$R_{12},R_{21}\ll R_{31},R_{32}\ll R_{13},R_{23}\ . \tag{4.2}$$

The consequence of the first inequality is that the direct charge transfer $2\leftrightarrow 1$ can be neglected in comparison with the optically induced transition via the transient state 3. The second inequality means that an excitation into the transient state 3 will be followed by immediate decay. State 3 will thus have only a negligible occupation probability.

The inequalities (4.2) allow an adiabatic elimination of the fast variable $\rho_{33}^{(0)}(t)$ in the pump-rate equation (2.14): The resulting two-state rate equation can be expressed in terms of the "spin" variable s:

$$\text{state } 1\triangleq s=-1\ ,\quad \text{state } 2\triangleq s=+1\ . \tag{4.3}$$

The variable s describes the dipole moment in units of d [see Eq. (3.1)]. The effective rate equation reads

$$\frac{d}{dt}\rho^{(0)}(s,t)=R_{-s}^{\text{eff}}\rho^{(0)}(-s,t)-R_s^{\text{eff}}\rho^{(0)}(s,t),\quad s=\pm 1\ . \tag{4.4}$$

$\rho^{(0)}(s,t)=\rho_{ss}^{(0)}(t)$, again, denotes the diagonal element. The effective rate R_s^{eff} for the indirect transition $s\rightarrow -s$ is

$$R_s^{\text{eff}}=\frac{W_{-s}}{W_1+W_{-1}}B_s U_{\text{pump}}(\omega_s^0)\ . \tag{4.5}$$

In our new notation we have set

$$\begin{aligned}
&W_{-1}=W_{13}\ ,\\
&W_1=W_{23}\ ,\\
&B_{-1}=B_{13}=B_{31}\ ,\\
&B_1=B_{23}=B_{32}\ ,\\
&\omega_{-1}^0=\omega_{31}^0=-\omega_{13}^0\ ,\\
&\omega_1^0=\omega_{32}^0=-\omega_{23}^0\ .
\end{aligned} \tag{4.6}$$

None of the other parameters apply.

For the mean dipole moment we get from (2.16), with the stationary solution of Eq. (4.4),

$$\bar{d}=d\frac{W_1B_{-1}U_{\text{pump}}(\omega_{-1}^0)-W_{-1}B_1U_{\text{pump}}(\omega_1^0)}{W_1B_{-1}U_{\text{pump}}(\omega_{-1}^0)+W_{-1}B_1U_{\text{pump}}(\omega_1^0)}\ . \tag{4.7}$$

Equation (4.7) shows that the two light modes $U_{\text{pump}}(\omega_{-1}^0)$ and $U_{\text{pump}}(\omega_1^0)$ compete with respect to the charge transfer: The first one tries to "switch" the dipole moment into direction $+d$, the second one into the reverse direction $-d$.[25] This is reminiscent of the excitatory and inhibitory forces typical for biological system control.

The susceptibility (2.22) contains comparable information: As the direct absorption $1\rightarrow 2$ can be neglected, the absorption spectrum consists of just two Lorentzians centered at ω_{31}^0 and ω_{32}^0. The peak heights are proportional to the corresponding occupation probabilities of the two states 1 and 2.

B. Cooperative network dynamics

In this section we consider a two-dimensional square array of interacting subsystems. We restrict our model in such a way that it can be mapped onto the kinetic Ising model.[33] This mapping is of twofold interest. On the one hand, the quantum network can be said to perform highly parallel Monte Carlo simulations as a possible application. On the other hand, well known results of the Ising model can be applied in order to get a better insight into the complex network dynamics.

If Eq. (4.1) is taken to hold for all subsystems m and all possible neighborhoods $\{i_n\}$, $n\neq m$,

$$\begin{aligned}
W_{31},W_{32},W_{21},W_{12}&\ll B_{i_mj_m}U_{\text{pump}}(\omega_{i_mj_m}(\{i_n\}),m)\\
&\ll W_{13},W_{23}
\end{aligned} \tag{4.8}$$

and for $i_mj_m=13$, 31, 23, and 32 a hierarchy in the total rates (2.25) results, corresponding to Eq. (4.2). An analogous adiabatic elimination procedure applied to Eq. (2.24) then gives an effective rate equation with two states per subsystem:

$$\begin{aligned}
\frac{d}{dt}\rho^{(0)}(s_1,s_2,\ldots,s_N;t)=\sum_{m=1}^{N}[&R_{-s_m}^{\text{eff}}(\{s_n\})\rho^{(0)}(s_1,s_2,\ldots,s_{m-1},-s_m,s_{m+1},\ldots,s_N;t)\\
&-R_{s_m}^{\text{eff}}(\{s_n\})\rho^{(0)}(s_1,s_2,\ldots,s_{m-1},s_m,s_{m+1},\ldots,s_N;t)]\ ,
\end{aligned} \tag{4.9}$$

where we have used the same nomenclature as in Sec. IV A. The effective rate $R_{s_m}^{\text{eff}}(\{s_n\})$ for the transition $s_m\rightarrow -s_m$ is

$$R_{s_m}^{\text{eff}}(\{s_n\})=\frac{W_{-s_m}}{W_1+W_{-1}}B_{s_m}U_{\text{pump}}[\omega_{s_m}(\{s_n\}),m]\ . \tag{4.10}$$

For the renormalized transition frequency $\omega_{s_m}\{(s_n\})$ we get from (2.23) with (3.1) and (3.4):

$$\omega_{s_m}(\{s_n\})=\omega_{s_m}^0-\sum_{\substack{n=1\\ n\neq m}}^{N}C_{mn}s_ms_n\ , \tag{4.11}$$

with

$$C_{mn}=\frac{d^2}{4\pi\epsilon\epsilon_0\hbar|\mathbf{R}_n-\mathbf{R}_m|^3}\ . \tag{4.12}$$

For $C(\mathbf{R}_n-\mathbf{R}_m)=C_{mn}$ we introduce the Fourier transform

$$\tilde{C}(\mathbf{k})=\sum_n C(\mathbf{R}_n-\mathbf{R}_m)\exp[-i\mathbf{k}(\mathbf{R}_n-\mathbf{R}_m)]\ , \tag{4.13}$$

$\tilde{C}(0)$ being the utmost frequency shift [cf. Eq. (4.11)] that can be induced by the neighborhood: Equation (4.11) defines two frequency bands of width $2\tilde{C}(0)$, centered around ω_{-1}^0 and ω_1^0. Under the condition

$$2\tilde{C}(0)<|\omega_1^0-\omega_{-1}^0|\ , \tag{4.14}$$

they do not overlap, and both directions of the transitions $s\leftrightarrow -s$ can be adjusted independently: For the spectral pump energy density $U_{\text{pump}}(\omega,m)$ we take the sum of two Gaussians with bandwidth Δ and detuning δ_s from the unperturbed transition frequencies ω_s^0, each confined to its respective band of transition energies:

$$U_{\text{pump}}(\omega,m)=\sum_{s=\pm1}U_s(m)\exp\left[-\left[\frac{\omega-\omega_s^0-\delta_s}{\Delta}\right]^2\right]\times\Theta[\tilde{C}(0)-|\omega-\omega_s^0|]\ . \tag{4.15}$$

As usual, the Θ function equals one for $\omega_s^0-\tilde{C}(0)<\omega<\omega_s^0+\tilde{C}(0)$, and zero otherwise. With Eqs. (4.15) and (4.11) the neighborhood-dependent transition rates (4.10) take the form

$$R_{s_m}^{\text{eff}}(\{s_n\})=\frac{W_{-s_m}}{W_{-1}+W_1}B_{s_m}U_{s_m}(m)\times\exp\left[-\left[\frac{\delta_{s_m}+\sum_{\substack{n=1\\n\neq m}}^{N}C_{mn}s_ms_n}{\Delta}\right]^2\right]\ . \tag{4.16}$$

The dynamics of the subsystems will be uncorrelated in the limit $\Delta\to\infty$. We will need the ratio

$$\frac{R_{s_m}^{\text{eff}}(\{s_n\})}{R_{-s_m}^{\text{eff}}(\{s_n\})}=\frac{W_{-s_m}B_{s_m}U_{s_m}(m)}{W_{s_m}B_{-s_m}U_{-s_m}(m)}\times\exp\left[-\frac{\delta_{s_m}^2-\delta_{-s_m}^2+2(\delta_{s_m}+\delta_{-s_m})\sum_{\substack{n=1\\n\neq m}}^{N}C_{mn}s_ms_n}{\Delta^2}\right] \tag{4.17}$$

for later reference. For an infinite square lattice, Eqs. (4.12) and (3.6) imply

$$\tilde{C}(0)=\sum_n C_{mn}=C_0\sum_{\substack{k,l=0\\(kl)\neq(00)}}^{\infty}\frac{1}{(k^2+l^2)^{3/2}}\approx 9.0336C_0\ . \tag{4.18}$$

With Eqs. (4.18), (3.5), and (3.6) we see that the inequality (4.14) is fulfilled in our model system.

We now take advantage of the fact that the type of rate equation (4.9) also governs the dynamics of the kinetic Ising model,[33,34] the Hamiltonian of which is given by

$$\hat{H}=-\sum_{m=1}^{N}\mu H_m s_m-\tfrac{1}{2}\sum_{\substack{m,n=1\\n\neq m}}^{N}J_{mn}s_ms_n\ . \tag{4.19}$$

Here, μ is the magnetic moment, H_m the local magnetic field, and $J_{mn}=J_{nm}$ is the exchange interaction between spin m and n. Coupling to a heat bath (temperature T) induces "spin flips" $s_m\to -s_m$. The principle of detailed balance,

$$R_{-s_m}^{\text{eff}}(\{s_n\})\rho^{(0)}(s_1,s_2,\ldots,s_{m-1},-s_m,s_{m+1},\ldots,s_N)=R_{s_m}^{\text{eff}}(\{s_n\})\rho^{(0)}(s_1,s_2,\ldots,s_{m-1},s_m,s_{m+1},\ldots,s_N)\ , \tag{4.20}$$

that holds for systems in thermal equilibrium,[35] determines the ratio

$$\frac{R_{s_m}^{\text{eff}}(\{s_n\})}{R_{-s_m}^{\text{eff}}(\{s_n\})}=\exp\left[-\frac{2}{k_BT}s_m\left[\mu H_m+\sum_{\substack{n=1\\n\neq m}}^{N}J_{mn}s_n\right]\right] \tag{4.21}$$

by a Boltzmann factor.[34]

Comparing the corresponding ratios of transition rates (4.17) with (4.21) yields the mapping

$$\frac{J_{mn}}{k_BT}=\frac{C_{mn}(\delta_1+\delta_{-1})}{\Delta^2}\ ,\qquad \frac{\mu H_m}{k_BT}=\tfrac{1}{2}\left[\ln\left[\frac{W_1B_{-1}U_{-1}(m)}{W_{-1}B_1U_1(m)}\right]+\frac{\delta_1^2-\delta_{-1}^2}{\Delta^2}\right]\ . \tag{4.22}$$

The mapping implies that the transition-rate model (4.16) also fulfills the condition of detailed balance (4.20), although it describes a driven system that is not in thermodynamic equilibrium. This is due to the special choice of the spectral energy density function (4.15).

Due to the mapping our quantum network can be considered as a "programmable" simulator of the kinetic Ising model. It is programmable in the sense that its parameters (J_{mn}/k_BT and $\mu H_m/k_BT$) can be adjusted by the external driving field: The intensity ratio $U_{-1}(m)/U_1(m)$ corresponds to the local magnetic field, the sign of the detuning parameter $\delta_1+\delta_{-1}$ determines ferromagnetic ($\delta_1+\delta_{-1}>0$) or antiferromagnetic coupling ($\delta_1+\delta_{-1}<0$). The application as an effective Monte Carlo simulator should have several advantages compared to conventional computers: First, the network

dynamics is highly parallel, i.e., the "computing time" does not depend on the size of the network. Second, quantum dynamics is intrinsically stochastic, whereas a conventional computer is deterministic and can only be made "quasistochastic" by special tricks. However, a lack of structural control leading to parameter fluctuations is connected with lacking control of the stochastic behavior and may induce systematic errors in the "random number generation." As another disadvantage, the distance dependence of the exchange interaction $J_{mn}=J(\mathbf{R}_n-\mathbf{R}_m)$ is determined by the R^{-3} distance dependence of the dipole-dipole interaction (4.12) and cannot be programmed at will as in a conventional computer. This, again, shows how physical limitations restrain the function of such a quantum device.

The two-dimensional Ising model (4.19) with $J_{mn}>0$ has a second-order phase transition from paramagnetism to ferromagnetism at a critical temperature T_c. Below T_c, a spontaneous magnetization occurs in zero magnetic field $H_m=0$. In the mean-field theory, the critical temperature is given by[36]

$$k_B T_c^{\mathrm{MF}}=\tilde{J}(0)\ , \tag{4.23}$$

where $\tilde{J}(0)$ is the Fourier transform of J_{mn} for $\mathbf{k}=0$ [cf. Eq. (4.13)].

The mapping (4.22) implies that the optically driven quantum network has a nonequilibrium phase transition at the critical pump parameter

$$\left[\frac{\tilde{C}(0)(\delta_1+\delta_{-1})}{\Delta^2}\right]_c^{\mathrm{MF}}=1\ . \tag{4.24}$$

Spontaneous polarization occurs for $\tilde{C}(0)(\delta_1+\delta_{-1})/\Delta^2>1$. Figure 3 shows the total dipole moment [$\hat{A}_m=\hat{d}_m$ in Eqs. (2.26), (2.27), and (2.32)] as a function of the bandwidth Δ for fixed parameter $\tilde{C}(0)$, detuning $\delta_1=\delta_{-1}=\tilde{C}(0)$ and zero magnetic field $U_{-1}(m)/U_1(m)=W_{-1}B_1/W_1B_{-1}$. From Eq. (4.24) we obtain for this choice $(\tilde{C}(0)/\Delta)_c^{\mathrm{MF}}=1/\sqrt{2}$. As expected from the exact solution of the two-dimensional Ising model with only nearest-neighbor interaction,[37] the mean-field value is lower than the exact value. This expectation is confirmed by our Monte Carlo simulation. However, the difference is not so large here as in[37] because the mean-field approximation tends to improve with the interaction range (it even becomes exact for infinite interaction range where each subsystem is coupled to any other with the same strength[38]).

Figure 4 shows typical dipole configurations, i.e., "snapshots" of the Monte Carlo simulation, for different parameters Δ. Qualitatively, these pictures resemble those of the nearest-neighbor Ising model.[38] $\tilde{C}(0)/\Delta=0$ corresponds to $T=\infty$: Each subsystem flips randomly without any correlation between the neighbors. For $\tilde{C}(0)/\Delta>0$ we get short-range order with clusters of aligned dipoles. The net dipole moment, however, remains zero until $\tilde{C}(0)/\Delta=[\tilde{C}(0)/\Delta]_c$. Then, the symmetry-breaking long-range order with spontaneous polarization appears until, for $\tilde{C}(0)/\Delta\to\infty$, the complete ordered state is reached.

The relevant level of description of the network dynamics requires the specification of the states s_n of all

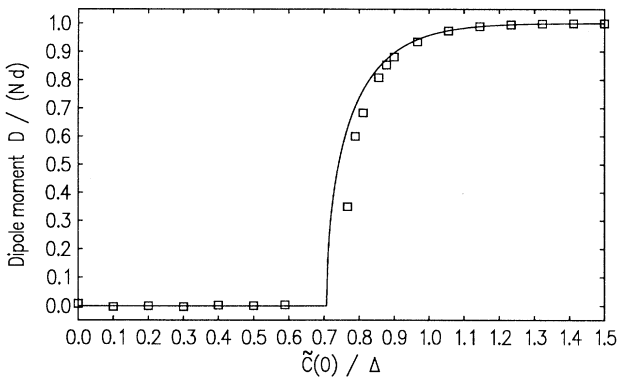

FIG. 3. Mean dipole moment vs inverse band width of the pump light field. Network of 40×40 subsystems, periodic boundary conditions. Fixed parameters $\delta_1=\delta_{-1}=\tilde{C}(0)$ and $U_{-1}(m)/U_1(m)=W_{-1}B_1/W_1B_{-1}$ (zero magnetic field). Squares, Monte Carlo simulation; continuous line, mean-field approximation. For clarity, only the positive-branch $D>0$ is shown. The complete picture is symmetric with respect to $D=0$.

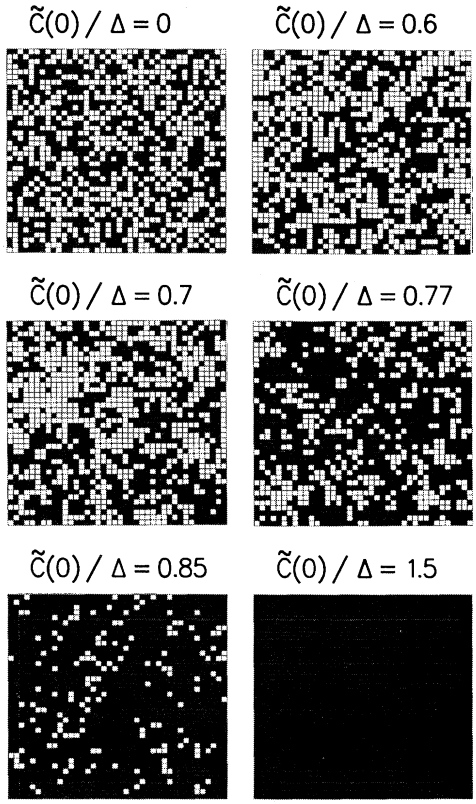

FIG. 4. Typical dipole configurations of the network (snapshots of Monte Carlo simulation). Black squares, $s=+1$; white squares, $s=-1$. Fixed parameters as in Fig. 3.

subsystems n. This detailed information shown in Fig. 4 will not be directly accessible to an actual physical experiment: Typical observational levels are not identical with the relevant level of the underlying network dynamics. This "reconstruction problem" appears to be typical for molecular electronics.

As an example, we illustrate a kind of "network analysis" through an absorption measurement. From Eq. (2.29) we get for the local susceptibility

$$\chi(\omega,m)=\frac{1}{\hbar\epsilon_0 v}\sum_{s_m}\sum_{\substack{\{s_n\}\\ n\neq m}}\frac{|d_{s_m}|^2(\omega_{s_m}(\{s_n\})-\omega-i\gamma_{s_m})}{(\omega_{s_m}(\{s_n\})-\omega)^2+\gamma_{s_m}^2}\times\rho^{(0)}(s_1,\ldots,s_N)\ . \tag{4.25}$$

and a corresponding expression for the total susceptibility (2.28). As in Eq. (4.6) we have introduced the abbreviations

$$\begin{aligned} &d_{-1}=d_{13}=d_{31}^*\ ,\\ &d_1=d_{23}=d_{32}^*\ ,\\ &\gamma_{-1}=\gamma_{13}=\gamma_{31}\ ,\\ &\gamma_1=\gamma_{23}=\gamma_{32}\ . \end{aligned} \tag{4.26}$$

Figure 5 shows the total absorption spectrum for the same parameters as in Fig. 4. We obtain two lines centered around the resonance frequencies ω_s^0 of the isolated subsystems, broadened and shifted due to the dipole-dipole interaction. The integral absorption over each line is proportional to the occupation probability of the corresponding state s [see Eq. (4.32) below]; their difference is thus proportional to the dipole moment as shown in Fig. 3. However, the specific line structure contains additional information: The broad-band absorption ("inhomogeneous line") for $\tilde{C}(0)/\Delta=0$ results from the uncorrelated neighborhood and the corresponding dynamical shift of the resonance frequency (see Sec. II C). The special line form is a consequence of the R^{-3} interaction. An infinite interaction range would lead to the usual Gaussian line. The cluster formation for increasing $\tilde{C}(0)/\Delta$ shows up as a shift of the absorption lines to lower frequencies [see Eq. (4.11)]. For $\tilde{C}(0)/\Delta > (\tilde{C}(0)/\Delta)_c$ one line starts to disappear due to the symmetry-breaking spontaneous polarization. For large enough $\tilde{C}(0)/\Delta$, one single "homogeneous" line remains as a consequence of the complete order state, where no fluctuations occur (on the observed time scale).

C. Programmable image processing

In the preceding section we focused on the dynamics of the quantum network itself. For the present application we consider the network as a "black box," while it is the connection between the absorption of the probe field and the controlling pump field that will be interpreted as a computer function. We will show that our network model is complex enough that this function can even be programmed although in a restricted manner. For this purpose we have to define "input", "output," and "program"

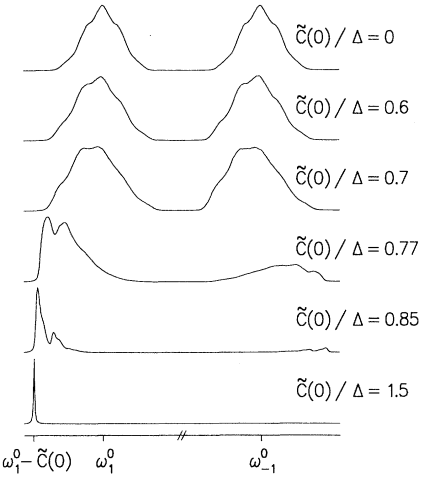

FIG. 5. Network absorption spectrum. Parameters as in Fig. 4. Homogeneous linewidths $\gamma_{-1}=\gamma_1=0.01\tilde{C}(0)$, transition dipole moments $|d_{-1}|^2=|d_1|^2$. For convenience, the spectra are normalized to equivalent peak height.

in our model: As in Eq. (4.15) we consider a spatially and frequency-dependent pump energy density. The spatially dependent part $\beta(m)$ as the "input pattern" is defined by

$$\beta(m)=A^{-1}\ln\left[\frac{W_1B_{-1}U_{-1}(m)}{W_{-1}B_1U_1(m)}\right], \tag{4.27}$$

where

$$A^2=\frac{1}{N}\sum_{m=1}^{N}\left[\ln\left[\frac{W_1B_{-1}U_{-1}(m)}{W_{-1}B_1U_1(m)}\right]\right]^2 \tag{4.28}$$

is a normalizing factor, so that

$$\frac{1}{N}\sum_{m=1}^{N}\beta(m)^2=1\ . \tag{4.29}$$

The mapping (4.22) shows that $\beta(m)$ is proportional to the local magnetic field H_m in the Ising model (for the case $\delta_1=\delta_{-1}$ as assumed in the following). We consider a spatially homogeneous probe light field with a frequency-dependent energy density $U_{\text{probe}}(\omega)$ which we parametrize by a cutoff Gaussian [cf. Eq. (4.15)]

$$U_{\text{probe}}(\omega)=U_{\text{probe}}^0\exp\left[-\left[\frac{\omega-\omega_1^0-\delta_{\text{probe}}}{\Delta_{\text{probe}}}\right]^2\right]\times\Theta[\tilde{C}(0)-|\omega-\omega_1^0|]\ . \tag{4.30}$$

The Θ function, here, assures that the probe field measures only absorption out of state $s=1$. The total (spatially dependent) absorption

$$\alpha(m)=-\int d\omega\, U_{\text{probe}}(\omega)\text{Im}\chi(\omega,m) \tag{4.31}$$

is defined as the "output pattern." Finally, the connection between input pattern $\beta(m)$ and output pattern $\alpha(m)$ is controlled by the program encoded in the parameters A (absolute intensity of the pump field), $\delta=\delta_1=\delta_{-1}$, Δ (frequency dependence of the pump field), and δ_{probe},

Δ_{probe} (frequency dependence of the probe field).

Our prototype input pattern is depicted in Fig. 6(a). For six program parameter sets we show computer simulations for the corresponding output patterns Figs. 6(b)–6(g). Figures 6(b)–6(e) examine the influence of the pump parameters: For $\tilde{C}(0)/\Delta_{\text{probe}}=0$ the probe energy density is frequency independent in the relevant range around ω_1^0 and $\alpha(m)$ measures the occupation probability

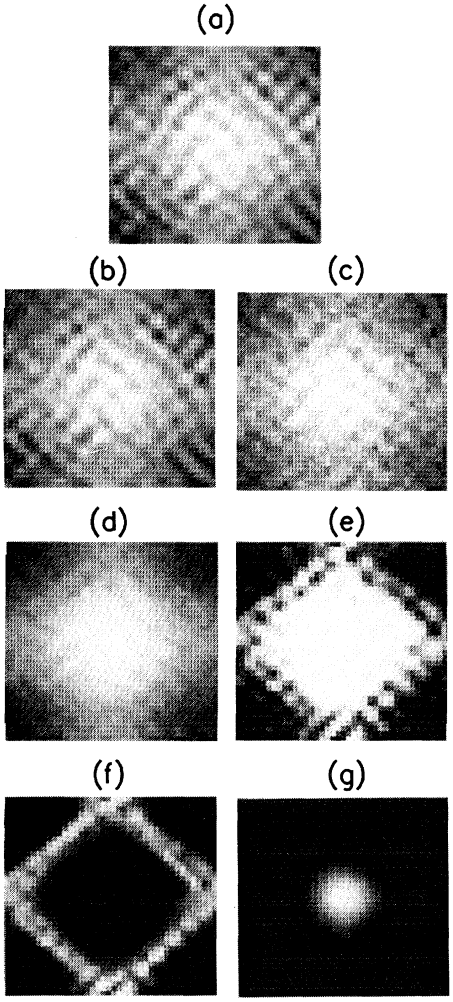

FIG. 6. Optical information processing by a network of 40×40 subsystems with periodic boundary conditions: Spatial pump intensity pattern $\beta(m)$ as input (a) and spatial absorption pattern $\alpha(m)$ as output (b)–(g) for different program parameters. Each computer simulation needed 5 h on a VAX station 4000/60. Light, $\alpha(m),\beta(m)$ large; dark, $\alpha(m),\beta(m)$ small. (b) $A=0.1$, $\delta/\tilde{C}(0)=1$, $\tilde{C}(0)/\Delta=0$, $\delta_{\text{probe}}/\tilde{C}(0)=0$, $\tilde{C}(0)/\Delta_{\text{probe}}=0$. (c) $A=0.1$, $\delta/\tilde{C}(0)=1$, $\tilde{C}(0)/\Delta=0.5$, $\delta_{\text{probe}}/\tilde{C}(0)=0$, $\tilde{C}(0)/\Delta_{\text{probe}}=0$. (d) $A=0.1$, $\delta/\tilde{C}(0)=1$, $\tilde{C}(0)/\Delta=0.7$, $\delta_{\text{probe}}/\tilde{C}(0)=0$, $\tilde{C}(0)/\Delta_{\text{probe}}=0$. (e) $A=2.0$, $\delta/\tilde{C}(0)=1$, $\tilde{C}(0)/\Delta=0.7$, $\delta_{\text{probe}}/\tilde{C}(0)=0$, $\tilde{C}(0)/\Delta_{\text{probe}}=0$. (f) $A=1.0$, $\delta/\tilde{C}(0)=1$, $\tilde{C}(0)/\Delta=0.7$, $\delta_{\text{probe}}/\tilde{C}(0)=0$, $\tilde{C}(0)/\Delta_{\text{probe}}=25$. (g) $A=1.0$, $\delta/\tilde{C}(0)=1$, $\tilde{C}(0)/\Delta=0.7$, $\delta_{\text{probe}}/\tilde{C}(0)=-1$, $\tilde{C}(0)/\Delta_{\text{probe}}=25$.

of state $s=1$, which depends linearly on the local dipole moment: From Eqs. (4.31), (4.30), (4.25), and (2.26) we get

$$\alpha(m)=\frac{\pi|d_1|^2U^0_{\text{probe}}}{2d\hbar\epsilon_0 v}(d+\langle\hat{d}_m\rangle)\ . \tag{4.32}$$

For $\tilde{C}(0)/\Delta=0$ [Fig. 6(b)] the dynamics of the subsystems is not coupled at all so that the response $\alpha(m)$ is local and, because the absolute input intensity is low, linear with $\beta(m)$. Increasing $\tilde{C}(0)/\Delta$ [Figs. 6(c) and 6(d)] leads to ferromagnetic coupling between the subsystems and smoothing of the output pattern. High input intensity [Fig. 6(e)] results in saturation effects: The output can be characterized as making a threshold decision $\beta(m)\gtrless0$. Finally, in Figs. 6(f) and 6(g) the effect of the probe parameters is investigated: The small probe band width $[\tilde{C}(0)/\Delta_{\text{probe}}=25]$ means that the absorption is sensitive to the local environment: In Fig. 6(f) (detuning $\delta_{\text{probe}}=0$) subsystems only absorb where the mean neighborhood dipole moment vanishes: This leads to the detection of the "edges" of our prototype pattern. In Fig. 6(g) [detuning $\delta_{\text{probe}}=-\tilde{C}(0)$] the probe beam is in resonance only with subsystems that are in the same state $s=1$ as their neighbors: In this way, the maximum of our input pattern is located. Local correlations (neighborhoods) are thus mapped into the response in frequency space. Furthermore, the network function is not determined by the internal dynamics alone (here, controlled by the pump field), as is the case in conventional computers; it is selected as well by the type of measurement (probe field).

Because of computer time limitations we could simulate only a small network (40×40 subsystems). Therefore, we have made the (unphysical) assumption that the light field ($\lambda\approx10^{-6}$ m) can vary on the scale of the network lattice constant ($a\approx10^{-7}$ m). For a more realistic model we would have to take at least a 100-times-larger system. The following arguments will show that the qualitative network properties should be independent of this scaling. However, there is no universal scaling law in the sense of renormalization theory.[39,40] The translation of the "program parameters" that connect a scaled input with a scaled output has to be check for each "function" separately.

For the smoothing function [Figs. 6(b)–6(d)], we again use mapping onto the Ising model. The mean-field theory predicts the following connection between the Fourier components of spin and magnetic field: For

$$\tilde{s}_{\mathbf{k}}=\sum_m s_m\exp(-i\mathbf{k}\cdot\mathbf{R}_m)\ , \tag{4.33}$$

and analogously for the magnetic field, we get for the linear response[36]

$$\frac{\langle\tilde{s}_{\mathbf{k}}\rangle}{\tilde{H}_{\mathbf{k}}}=\frac{\mu}{k_BT-\tilde{J}(\mathbf{k})}\ . \tag{4.34}$$

With $J(\mathbf{R}_n-\mathbf{R}_m)=J_0a^3/|\mathbf{R}_n-\mathbf{R}_m|^3$ (nearest-neighbor interaction J_0) one obtains in the limit $|\mathbf{k}|a\ll1$

$$\tilde{J}(\mathbf{k})=\tilde{J}(0)-2\pi J_0a|\mathbf{k}|\ . \tag{4.35}$$

Inserting this expression into (4.34) gives

$$\frac{\langle \tilde{s}(\mathbf{k}) \rangle}{\tilde{H}(\mathbf{k})} = \frac{\mu}{2\pi J_0 a} \frac{1}{\xi^{-1} + |\mathbf{k}|} , \tag{4.36}$$

with

$$\xi = \frac{2\pi J_0 a}{k_B (T - T_c^{\mathrm{MF}})} . \tag{4.37}$$

Wavelengths smaller than the spin-spin correlation length ξ are damped. As $\tilde{\alpha}(\mathbf{k}) \sim \tilde{s}_{\mathbf{k}}$ for $\tilde{C}(0)/\Delta_{\mathrm{probe}} = 0$ [following from Eq. (4.32)] and $\tilde{\beta}(\mathbf{k}) \sim \tilde{H}_{\mathbf{k}}$, this means for our pump and probe experiment that the output pattern will average out the input pattern on a length scale ξ that increases by approaching the critical parameter $[\tilde{C}(0)/\Delta]_c$, as observed in Figs. 6(b)–6(d). Inserting the mapping (4.22) into (4.37) establishes a "scaling law" for the program parameters $\delta_{\pm 1}$ and Δ in this application.

For the other applications [Figs. 6(e)–6(g)], not the long-range correlation ξ but local saturation and neighborhood are decisive. These features should be independent of a scaling of the system and thus the corresponding functions are expected to survive without parameter scaling.

V. SUMMARY AND CONCLUSIONS

The challenge of molecular electronics is the realization of synthetic nanostructures capable of performing a computer function. We have pointed out that computational aspects and physical implementation should be combined in this field rather than treated independently. Driven by an external light field, our quantum network model performs complex stochastic dynamics. This has been explicitly demonstrated for the kinetic Ising model with $J(\mathbf{R}_n - \mathbf{R}_m) \sim |\mathbf{R}_n - \mathbf{R}_m|^{-3}$, where the quantum network carries out a highly parallel Monte Carlo calculation and results are obtained directly as physical measurements. With a conventional computer this could only be achieved with time-consuming simulations (which we actually did to obtain our results). In a second application we have demonstrated how simple image-processing tasks can be programmed and directly performed by pump and probe experiments.

There are two difficulties in these applications for molecular electronics: First, on the quantum level primitive functions are constrained, e.g., the coupling constants J_{mn} of the Ising model cannot be chosen at will, since their distance dependence is restricted by the R^{-3} law of the dipole-dipole interaction. In our second application, a set of "program parameters" can be assigned to a certain function, but the reverse problem of algorithmically finding the parameters for a given function, remains unsolved. This appears to be a typical problem of many new computer concepts. For the cellular automaton, e.g., which was originally introduced to model physical, chemical, and biological systems,[41] general statements about its computational universality exist,[42] which, however, are rarely of practical use. In typical applications (e.g., for lattice gas models[43]), the automaton rules are established in a rather intuitive manner. In this same spirit one may investigate to what extent quantum networks could be used to model emergent behavior of other (physical) systems. It seems likely that such a quantum computer will be applied as a special- rather than a general-purpose machine, but then, as shown, with very high efficiency.

ACKNOWLEDGMENT

This work has been supported in part by the Deutsche Forschungsgemeinschaft (Sfb 329).

[1]See, e.g., R. C. Haddon and A. A. Lamola, Proc. Natl. Acad. Sci. U.S.A. **82**, 1874 (1985).
[2]T. S. Arrhenius *et al.*, Proc. Natl. Acad. Sci. U.S.A. **83**, 5355 (1986).
[3]F. L. Carter, *Molecular Electronic Devices* (Dekker, New York, 1982).
[4]F. L. Carter, *Proceedings of the Second International Workshop on Molecular Electronic Devices* (Dekker, New York, 1987).
[5]A. Aviram and M. Ratner, Chem. Phys. Lett. **29**, 277 (1974).
[6]A. L. Robinson, Science **220**, 940 (1983).
[7]J. J. Hopfield, Proc. Natl. Acad. Sci. U.S.A. **79**, 2554 (1982).
[8]H. Mühlenbein, M. Gorges-Schleuter, and O. Krämer, Parallel Computing **6**, 269 (1987).
[9]S. Wolfram, Physica D **10**, 1 (1984).
[10]L. J. Geerligs *et al.*, Phys. Rev. Lett. **64**, 2691 (1990).
[11]G. Schulz-Ekloff, in *Zeolite Chemistry and Catalysis,* edited by P. A. Jacobs *et al.* (Elsevier, Amsterdam, 1991), p. 65.
[12]W. Nagourney, J. Sandberg, and H. Dehmelt, Phys. Rev. Lett. **56**, 2797 (1986).
[13]Th. Sauter, W. Neuhauser, R. Blatt, and P. E. Toschek, Phys. Rev. Lett. **57**, 1696 (1986).
[14]J. C. Berquist, R. G. Hulet, W. M. Itano, and D. J. Wineland, Phys. Rev. Lett. **57**, 1699 (1986).
[15]M. Orrit and J. Bernard, Phys. Rev. Lett. **65**, 2716 (1990).
[16]Th. Sauter, R. Blatt, W. Neuhauser, and P. E. Toschek, Opt. Commun. **60**, 287 (1986).
[17]W. P. Ambrose and W. E. Moerner, Nature **349**, 225 (1991).
[18]K. R. Farmer, C. T. Rogers, and R. A. Buhrman, Phys. Rev. Lett. **58**, 2255 (1987).
[19]P. Reineker, in *Exciton Dynamics in Molecular Crystals and Aggregates,* edited by G. Höhler, Springer Tracts in Modern Physics, Vol. 94 (Springer, Berlin, 1982).
[20]K. Blum, *Density Matrix Theory and Applications* (Plenum, New York, 1981).
[21]Y. R. Shen, *The Principles of Nonlinear Optics* (Wiley, New York, 1984).
[22]R. Loudon, *The Quantum Theory of Light,* 2nd ed. (Clarendon, Oxford, 1983).
[23]W. G. Teich and G. Mahler, Phys. Rev. A **45**, 3300 (1992).
[24]M. J. Kirton and M. J. Uren, Adv. Phys. **38**, 367 (1989).
[25]K. Obermayer, W. G. Teich, and G. Mahler, Phys. Rev. B **37**, 8096 (1988).
[26]M. Mehring, in *Electronic Properties of Conjugated Polymers,* edited by H. Kuzmany, M. Mehring, and S. Roth (Springer, Heidelberg, 1989).
[27]H. Körner and G. Mahler, Phys. Rev. Lett. **65**, 984 (1990).

[28]G. Mahler, H. Körner, and W. Teich, in *Festkörperprobleme / Advances in Solid State Physics,* edited by U. Rössler (Vieweg, Braunschweig, 1991), Vol. 31, p. 357.
[29]M. G. W. Alexander *et al.*, Appl. Phys. Lett. **55**, 885 (1989).
[30]M. A. Reed *et al.*, Phys. Rev. Lett. **60**, 535 (1988).
[31]W. G. Teich, K. Obermayer, and G. Mahler, Phys. Rev. B **37**, 8111 (1988).
[32]K. Heldmann, W. G. Teich, and G. Mahler, Phys. Rev. B **44**, 3829 (1991).
[33]R. J. Glauber, J. Math. Phys. **4**, 294 (1963).
[34]M. Suzuki and R. Kubo, J. Phys. Soc. Jpn. **24**, 51 (1968).
[35]H. Haken, *Synergetics. An Introduction,* 3rd ed. (Springer, Berlin, 1983).
[36]R. Brout, *Phase Transitions* (Benjamin, New York, 1965).
[37]L. Onsager, Phys. Rev. **65**, 117 (1944).
[38]H. E. Stanley, *Introduction to Phase Transitions and Critical Phenomena* (Clarendon, Oxford, 1971).
[30]S. K. Ma, *Modern Theory of Critical Phenomena* (Benjamin, London, 1976).
[40]J. J. Binney *et al.*, *The Theory of Critical Phenomena* (Clarendon, Oxford, 1992).
[41]J. von Neumann, *The Theory of Self-Reproducing Automata,* edited by A. W. Burks (University of Illinois Press, Urbana, 1966).
[42]J. Albert, K. Culik II, Complex Systems **1**, 1 (1987).
[43]U. Frisch, B. Hasslacher, and Y. Pomeau, Phys. Rev. Lett. **56**, 1505 (1986).

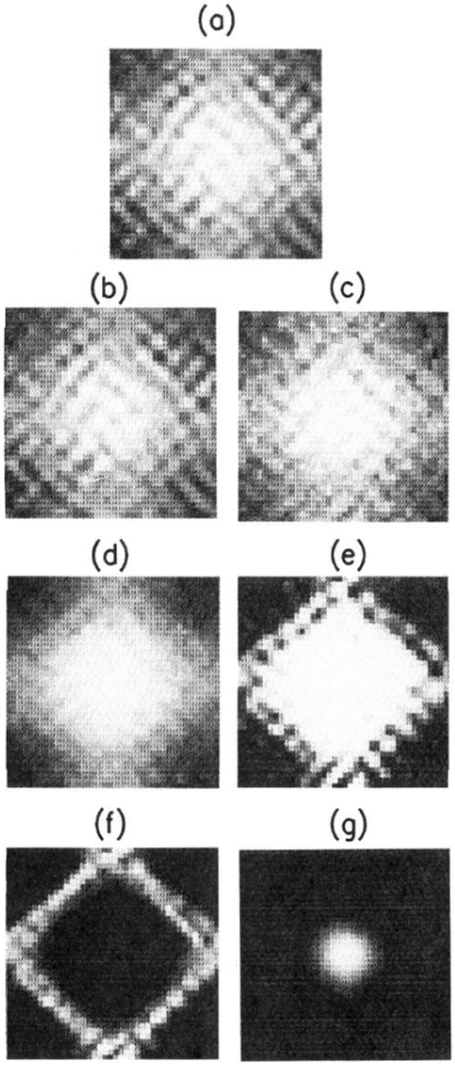

FIG. 6. Optical information processing by a network of 40×40 subsystems with periodic boundary conditions: Spatial pump intensity pattern $\beta(m)$ as input (a) and spatial absorption pattern $\alpha(m)$ as output (b)–(g) for different program parameters. Each computer simulation needed 5 h on a VAX station 4000/60. Light, $\alpha(m),\beta(m)$ large; dark, $\alpha(m),\beta(m)$ small. (b) $A=0.1$, $\delta/\tilde{C}(0)=1$, $\tilde{C}(0)/\Delta=0$, $\delta_{\text{probe}}/\tilde{C}(0)=0$, $\tilde{C}(0)/\Delta_{\text{probe}}=0$. (c) $A=0.1$, $\delta/\tilde{C}(0)=1$, $\tilde{C}(0)/\Delta=0.5$, $\delta_{\text{probe}}/\tilde{C}(0)=0$, $\tilde{C}(0)/\Delta_{\text{probe}}=0$. (d) $A=0.1$, $\delta/\tilde{C}(0)=1$, $\tilde{C}(0)/\Delta=0.7$, $\delta_{\text{probe}}/\tilde{C}(0)=0$, $\tilde{C}(0)/\Delta_{\text{probe}}=0$. (e) $A=2.0$, $\delta/\tilde{C}(0)=1$, $\tilde{C}(0)/\Delta=0.7$, $\delta_{\text{probe}}/\tilde{C}(0)=0$, $\tilde{C}(0)/\Delta_{\text{probe}}=0$. (f) $A=1.0$, $\delta/\tilde{C}(0)=1$, $\tilde{C}(0)/\Delta=0.7$, $\delta_{\text{probe}}/\tilde{C}(0)=0$, $\tilde{C}(0)/\Delta_{\text{probe}}=25$. (g) $A=1.0$, $\delta/\tilde{C}(0)=1$, $\tilde{C}(0)/\Delta=0.7$, $\delta_{\text{probe}}/\tilde{C}(0)=-1$, $\tilde{C}(0)/\Delta_{\text{probe}}=25$.